Systematic study of electrochemical performance of nickel iron hydroxide (NiFe(OH)2) electrocatalyst at high current densities in alkaline seawater solutions

Jack Corbin [a], Cheng Lyu [a], David Trudgeon [a], Mikey Jones [a], Adeline Loh [a], Arthur Graf [b], Zhenyu Zhang [a], Jianyun Cao [c], Ida Nawrocka [a], Xiaohong Li [a*]

Appendix/supporting information for 1st research chapter.

Table S1: ECSA and roughness factor calculations of Ni microelectrode in 1 M KOH at 293K.

Synthesis parameters	**Cdl (Farads)**	**ECSA calculated using established C_s (20 µF cm^{-2}) for Nickel (cm^2)**	**Roughness factor, R_f**	**ECSA calculated using ME Cdl (cm^2)** (Example: 1.728 × 10^{-8} / 4.909 x 10^{-6} = 3.52 x 10^{-3})	**Roughness factor, R_f**
Uncoated microelectrode	**1.728 × 10^{-8}**	0.01728/20 = **8.639 x 10^{-4} = 0.00086394 cm^2**	8.639 x 10^{-4} /4.909x10^{-6} = 175.99 = 176	**1.728 × 10^{-8}/3.52 x 10^{-3} = 4.909 x 10^{-6} cm^2**	**4.909 x 10^{-6} / 4.909 x 10^{-6} = 1**
NiFe(OH)$_2$ coated microelectrode at 2.5 mA cm^{-2} for 5000 s	**1.446 × 10^{-8}**	0.01446/20 = **7.23 x 10^{-4}**	**7.23 x 10^{-4}** /4.909x10^{-6} = 147.28	**1.446 × 10^{-8}/3.52 x 10^{-3} = 4.108 x 10^{-6} cm^2**	**4.108 x 10^{-6} / 4.909 x 10^{-6} = 0.836**
NiFe(OH)$_2$ coated microelectrode at 25 mA cm^{-2} for 500 s	**1.942 × 10^{-8}**	0.01942/20 = **9.71 x 10^{-4}**	**9.71 x 10^{-4}**/4.909x10^{-6} = 197.79	**1.942 × 10^{-8}/3.52 x 10^{-3} = 5.517 x 10^{-6} cm^2**	**5.517 x 10^{-6} / 4.909 x 10^{-6} = 1.123**
NiFe(OH)$_2$ coated microelectrode at 250 mA cm^{-2} for 50 s	**2.712 × 10^{-8}**	0.02712/20 = **1.356 x 10^{-3}**	**1.356 x 10^{-3}** /4.909x10^{-6} = 276.22	**2.712 × 10^{-8}/ 3.52 x 10^{-3} = 7.704 x 10^{-6} cm^2**	**7.704 x 10^{-6} / 4.909 x 10^{-6} = 1.569**

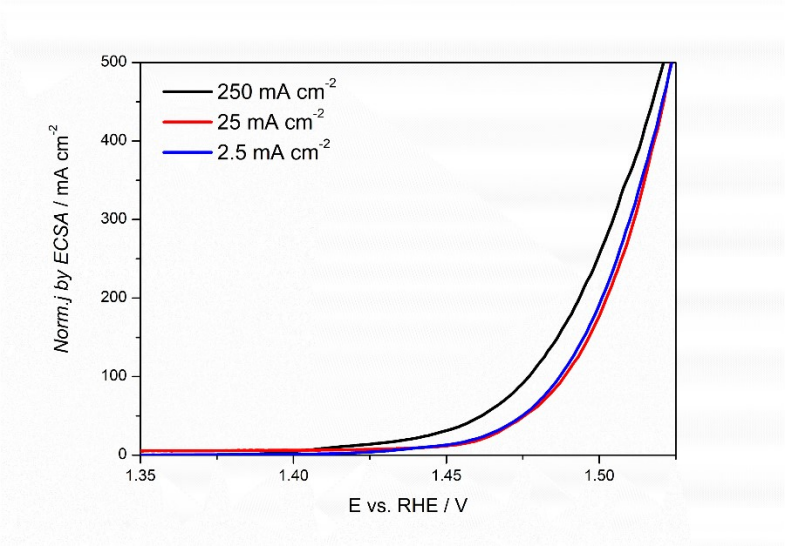

Fig. S1 Corresponding electrochemical performance of Ni microelectrode synthesised using different electrodeposition current densities normalised by ECSA in 1 M KOH at 333K at a scan rate of 1 mV s^{-1}.

Temperature coefficient formula [1] (mV/K):

$$E_T^0 = E_{298K}^{\ 0} + (T - 298K) \times \left(\frac{dE^0}{dT}\right)_{298}$$

In alkaline media, ClO^-

E^0 = 0.890 V at 298K, -1.08 dE^0/dT (mV/k) (S1)

$E_T^0 = 0.890 + (333K - 298K) \times (-1.08)_{298} = -36.91$ mV/K (S2)

∴ 890 mV – 36.91 mV = 853.09 mV (S3)

In alkaline media, OER

E^0 = 0.4011 V at 298K, -1.6816 dE^0/dT (mV/k) (S4)

$E_T^0 = 0.4011 + (333 - 298K) \times (-1.6816)_{298} = -58.45$ mV/K (S5)

∴ 401 mV – 58.45 mV = 342.55 mV (S6)

∴ ClO^- - OER at 333K = 853.09 mV – 342.55 mV = 511 mV at 333K (S7)

Simplified Nernst equation for converting to RHE

$$E_{RHE} = E_{Hg/HgO} + \left(2.303 \times \frac{RT}{F}\right) \times pH + E_{Hg/HgO}^{\ 0} \quad \text{(S8)}$$

R is the ideal gas constant (8.314 J K^{-1} mol^{-1}), T is the temperature (293 K), F is the Faraday constant (96485 C mol^{-1}), and $E^0_{Hg/HgO}$ is the standard potential of the Hg/HgO electrode

(0.0983 V vs. standard hydrogen electrode). All potentials are quoted vs. RHE unless otherwise stated.

Table S2: Composition of seawater using ~35 PSU.[1] Composition of Absolute Ocean (AbsOcean) standardised seawater solution using the concentration of each element, provided by the supplier ATI-Aquaristik.

Element	Chemical formula	Concentration (mg/L)	Composition as % of total	AbsOcean Concentration (mg/L^{-1})	Deviation (%)	Trace elements (µg/L)	Deviation (%)
Chloride	Cl^-	19000	54.95	19800	2	Lithium (172)	10
Bromide	Br^-	67	0.19	68	2	Rubidium (120)	10
Sulfate	SO_4^{2-}	2700	7.8	925	2	Iodine (70)	4
Fluoride	F^-	1.3	0.00	1.3	2	Molybdenum (12)	2
Bicarbonate	HCO_3^-	142	0.41	-	2	Barium (10)	2
Calcium	Ca^+	410	1.16	421	2	Vanadium (1.4)	0.4
Magnesium	Mg^+	1350	3.90	1313	2	Zinc (1)	0.4
Boric acid	H_3BO_3	4.5	0.07	4.5	2		
Strontium	Sr^{2+}	8	0.04	8.1	2		
Sodium	Na^+	10500	30.37	11035	2		
Potassium	K^+	390	1.12	408	2		
Total	-	34,572	99.99	34,370 (inc. trace)	2		

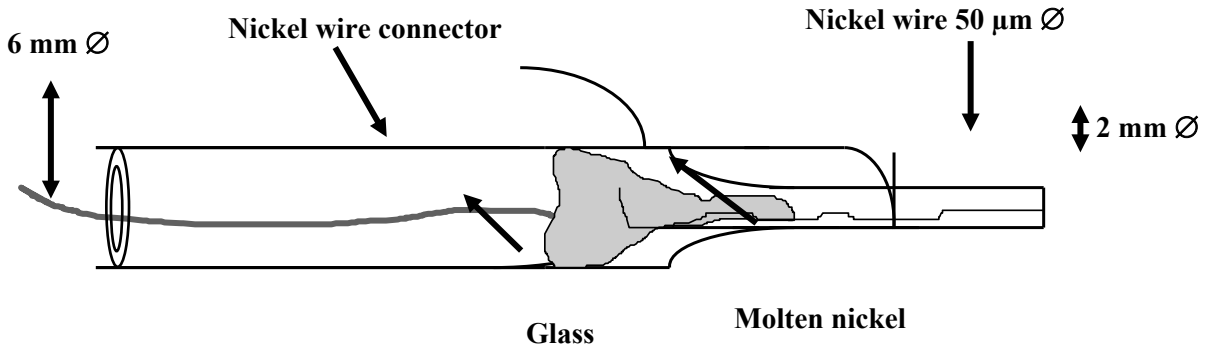

Fig. S2 Microelectrode schematic.

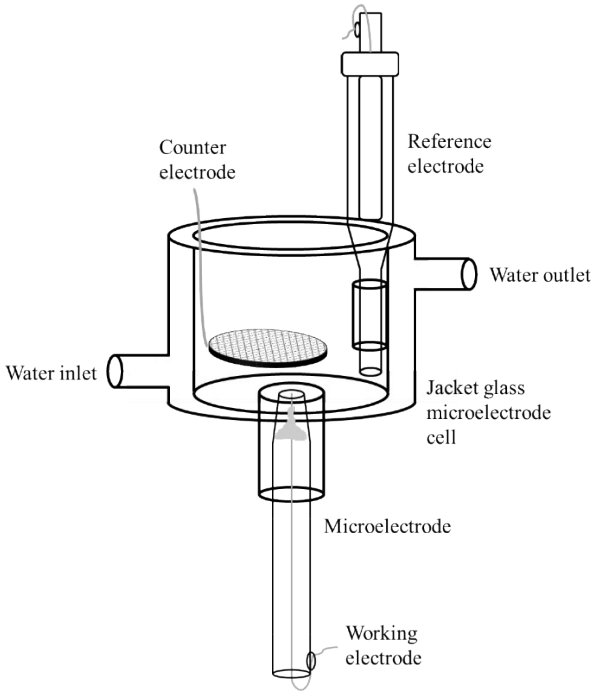

Fig. S3 ME setup for electrochemical testing of the $NiFe(OH)_2$.

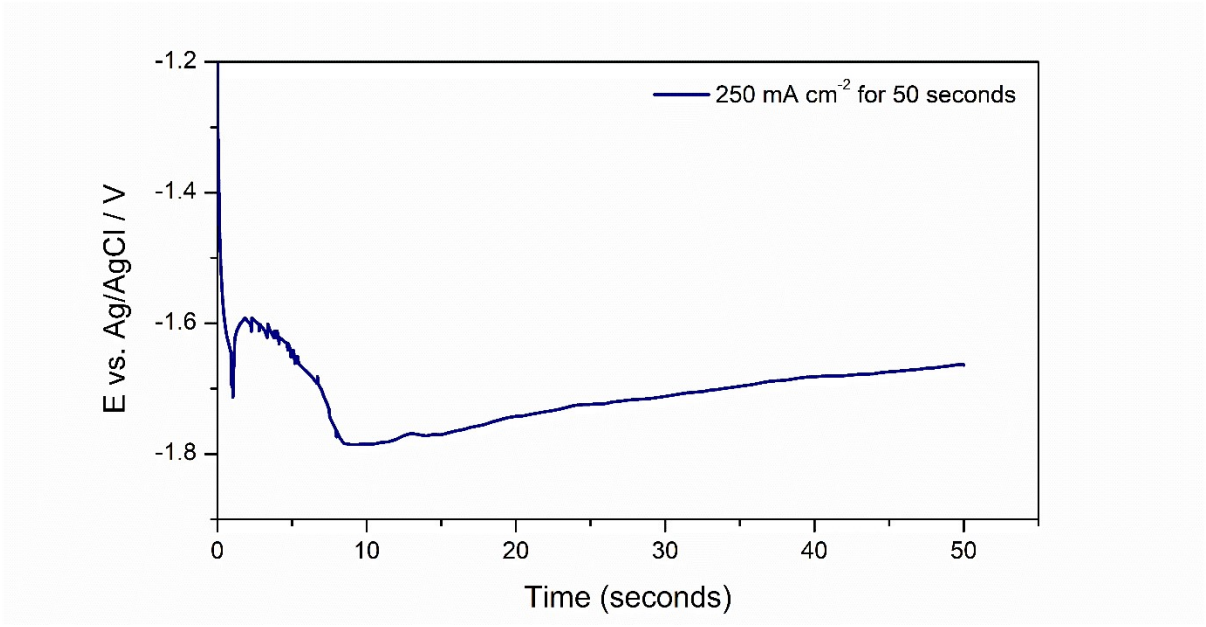

Fig S4: Chronopotentiometry electrodeposition experiment within 18 mM metal sulphate & 25 mM ammonium sulphate at a current density of 250 mA cm^{-2} over 50 seconds on a Ni ME diameter 50 µm at room temperature.

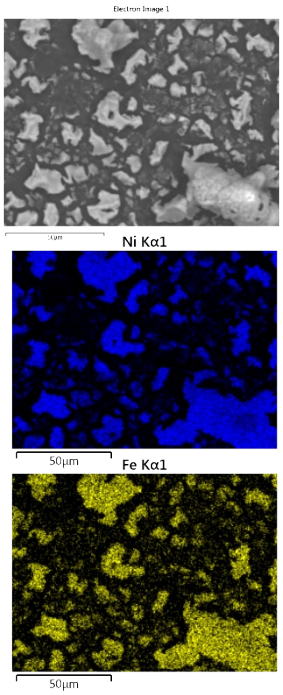

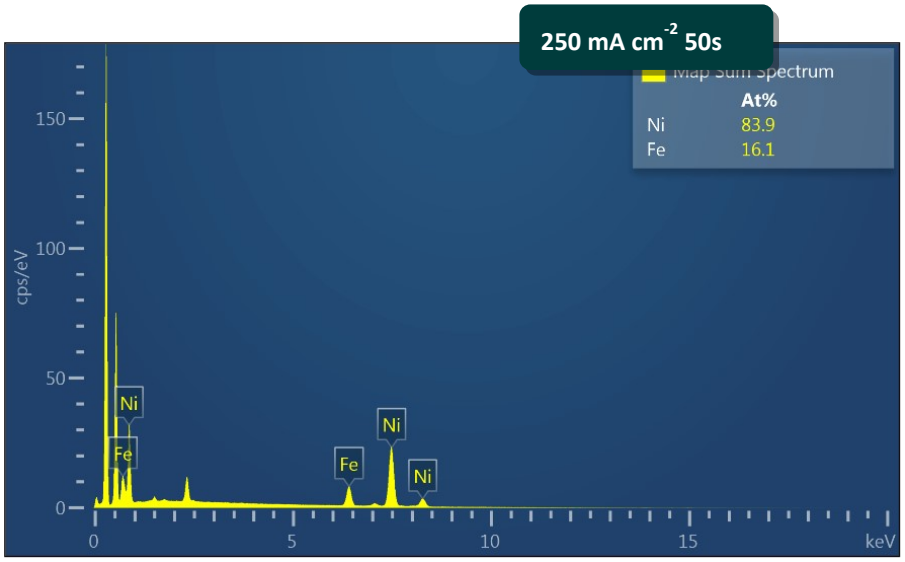

Fig. S5 EDS plot of $NiFe(OH)_2$ catalyst synthesised using 250 mA cm^{-2} for 50 seconds on polished carbon plate, 1 cm^2 surface area within 18 mM metal sulphate & 25 mM ammonium sulphate.

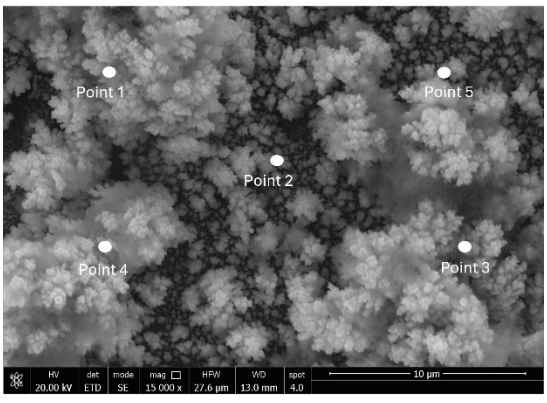

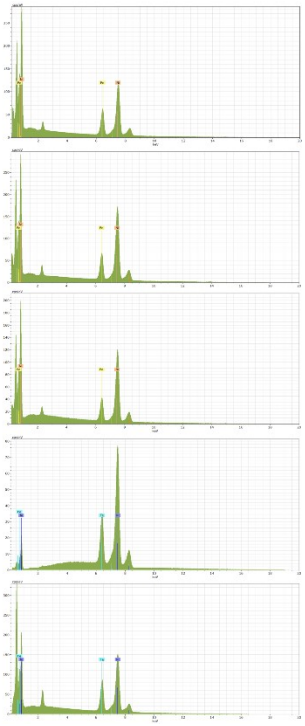

Element	Point 1	Point 2	Point 3	Point 4	Point 5	Average
Iron	21.37199	16.56663	20.13593	21.35361	18.26666	19.53896
Nickel	78.62801	83.43337	79.86407	78.64639	81.73334	80.46104

Fig. S6 EDS plot of $NiFe(OH)_2$ catalyst synthesised using 25 mA cm^{-2} for 500 seconds on polished carbon plate, 1 cm^2 surface area within 18 mM metal sulphate & 25 mM ammonium sulphate.

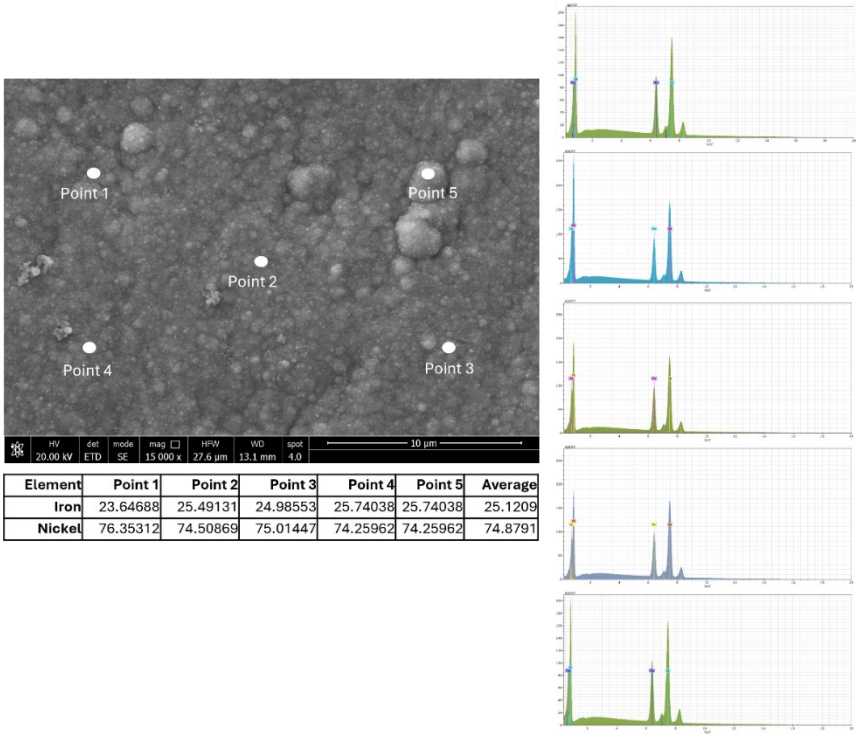

Element	Point 1	Point 2	Point 3	Point 4	Point 5	Average
Iron	23.64688	25.49131	24.98553	25.74038	25.74038	25.1209
Nickel	76.35312	74.50869	75.01447	74.25962	74.25962	74.8791

Fig. S7 EDS plot of $NiFe(OH)_2$ catalyst synthesised using 2.5 mA cm^{-2} for 5000 seconds on polished carbon plate, 1 cm^2 surface area within 18 mM metal sulphate & 25 mM ammonium sulphate.

Braggs Law

$$n\lambda = 2dsin(\theta) \quad \text{(S9)}$$

where λ = wavelength of the X-ray beam (0.154nm), d = spacing between adjacent crystal sheets/layers, n is an integer and θ is the diffraction angle.

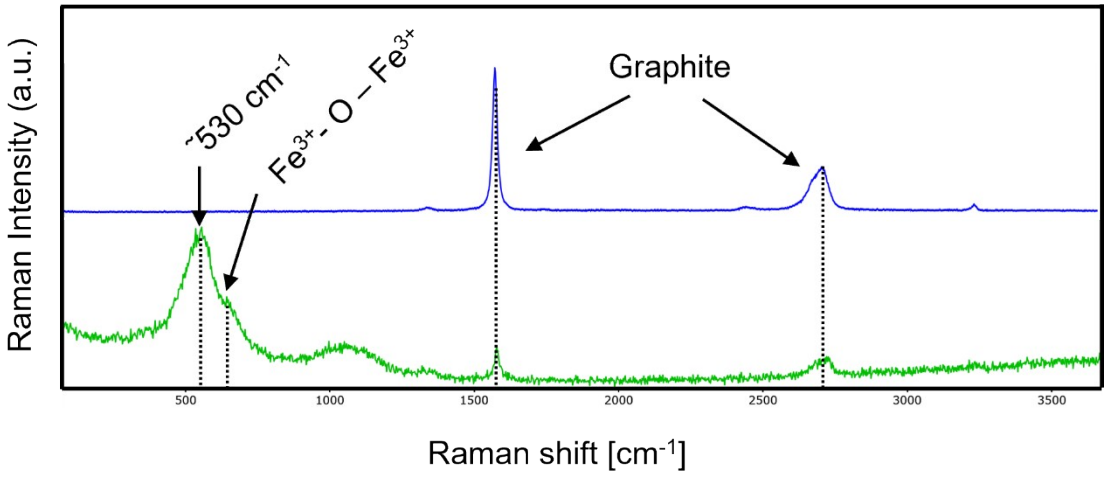

Fig. S8 Raman spectroscopy peaks for bare carbon plate (blue line) and $NiFe(OH)_2$ coated carbon plate, surface area 1 cm^2.

Fig. S9 a) Preparing 500 ml of 1 M KOH and unfiltered natural seawater, pH 13.9. After the addition of KOH base, a white precipitate is observed in the solution, which is mainly composed of $Mg(OH)_2$ and $Ca(OH)_2$ which is widely reported in literature [2] b & c) 1 M KOH and unfiltered natural seawater 24 hours after preparation with the $Mg(OH)_2$ and $Ca(OH)_2$ at the bottom of the solution.

It is worth highlighting that when adding KOH to the seawater to create the electrolyte, spontaneous precipitation of alkaline earth carbonates and hydroxides occurs within the solution as a result of the local pH increase, creating a cloudy appearance (Fig. S8a).[2] A negligible drop in conductivity is observed between the states of the electrolytes (194.4 mS/cm

vs 193.2 mS/cm). After a couple of hours, these precipitates will sink to the bottom of the solution (Fig. S10 b&c), and the transparent buffered seawater electrolyte can be syphoned out accordingly. In the context of alkaline earth metals (Mg^{2+} and Ca^{2+}), the corresponding hydroxides and carbonates with low solubility in alkaline media present a detrimental impact on the properties of electrodes and membranes within a seawater electrolyser, such as physical blockage to active sites and electron pathways. To mitigate this, some studies have introduced Mass transport channels on the surface of cathode catalysts, which provide a quick pathway for the movement of bubbles, fluids, and precipitates, helping prevent their accumulation on the electrode surface, accelerating the mass transport steps involved in the HER process, and enhancing HER stability. [3,4]

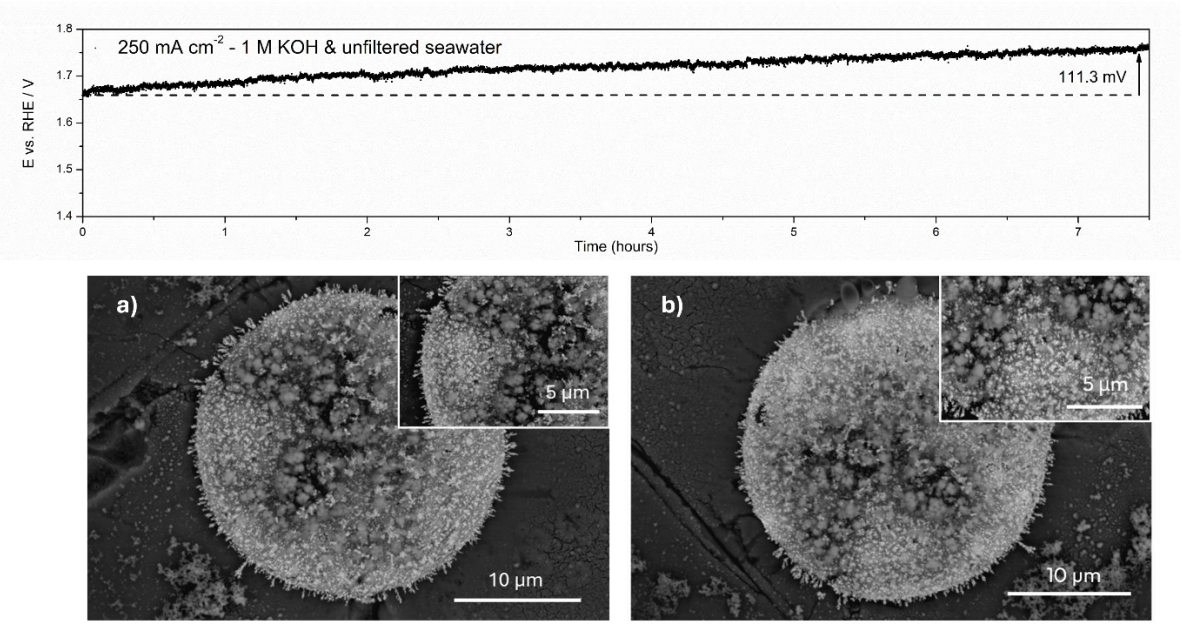

Fig. S10 CP long-term stability test $NiFe(OH)_2$ coated Pt microelectrode, diameter 25 µm in 1 M KOH & natural seawater at 293 K at a constant current of 250 mA cm^{-2} for 7.5 hours a) SEM image of $NiFe(OH)_2$ deposited on Pt microelectrode, diameter 25 µm within 18 mM metal sulphate & 25 mM ammonium sulphate using cathodic electrodeposition at 250 mA cm^{-2} for 50 seconds before alkaline natural seawater testing b) SEM image of $NiFe(OH)_2$ deposited on Pt microelectrode, diameter 25 µm, after 7.5 hours at 293K and 250 mA cm^{-2} in alkaline natural seawater (1 M KOH & unfiltered seawater).

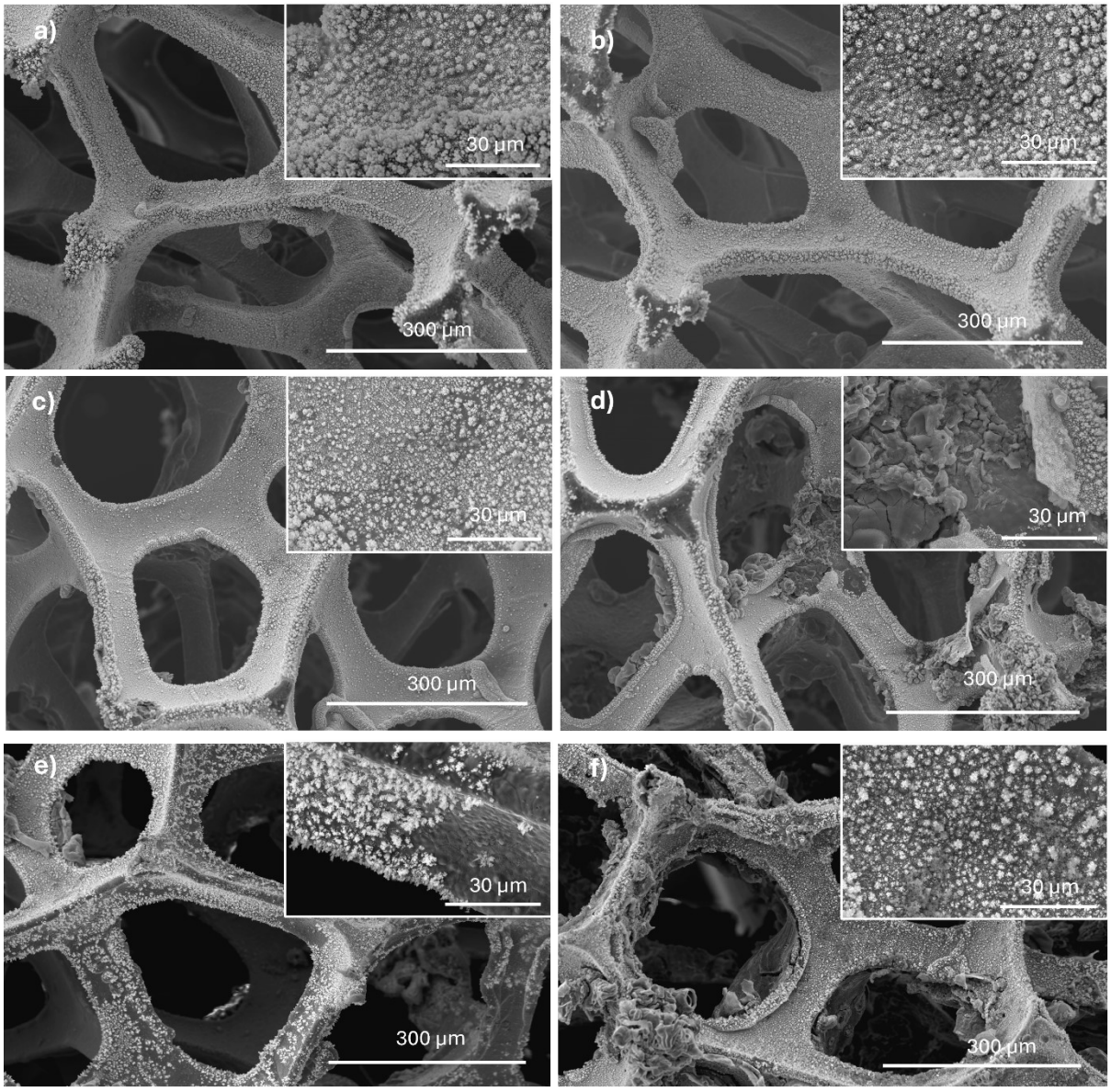

Fig. S11 SEM images of $NiFe(OH)_2$ deposited at 25 mA cm^{-2} on Ni foam a) pristine sample b) sample after 10h of electrolysis in 1 M KOH c – d) sample after 10h of electrolysis in 1 M KOH & AbsOcean e – f) sample after 10h of electrolysis in 1 M KOH & unfiltered seawater.

Table S3 EDS results of CP stability tests of $NiFe(OH)_2$ in varying electrolytes.

	Element	Point 1	Point 2	Point 3	Average	Retention vs. pristine (%)
Pristine $NiFe(OH)_2$	**Iron**	4.44	4.39	4.52	4.45	N/A
	Nickel	95.55	95.60	95.47	95.54	
$NiFe(OH)_2$ after 10h KOH	**Iron**	1.08	3.83	2.12	2.34	-47.41
	Nickel	98.91	96.16	97.76	97.61	+2.16
$NiFe(OH)_2$ after 10h KOH & AbsOcean	**Iron**	1.92	1.77	3.02	2.23	-49.88
	Nickel	98.07	98.22	96.97	97.75	+2.31
$NiFe(OH)_2$ after 10h KOH & unfiltered seawater	**Iron**	1.89	3.49	1.62	2.33	-47.64
	Nickel	98.10	96.50	98.37	97.65	+2.20

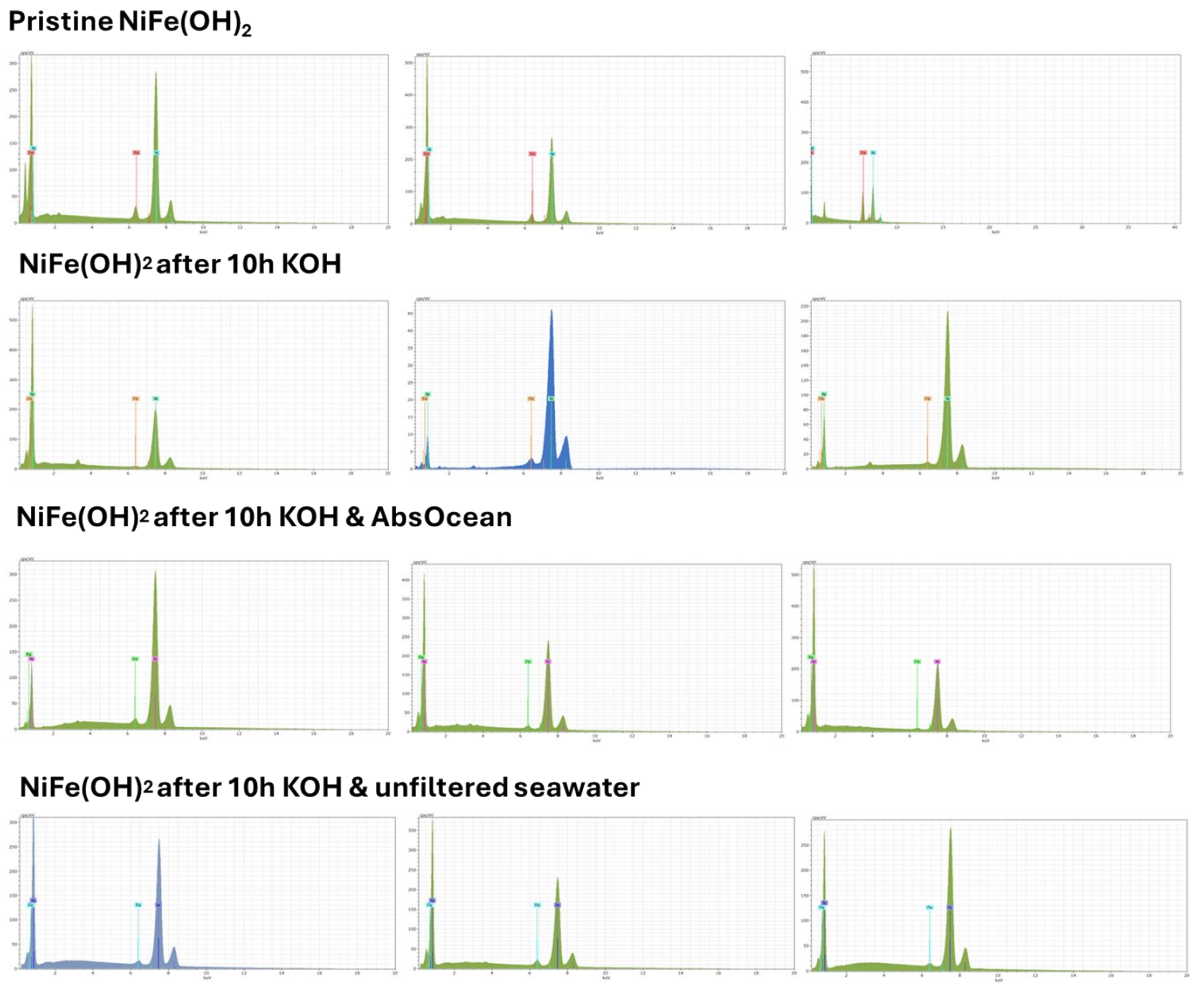

Fig. S12 EDS spectra's of $NiFe(OH)_2$ after testing in varying electrolytes at 100 mA cm^{-2} for 10 h.

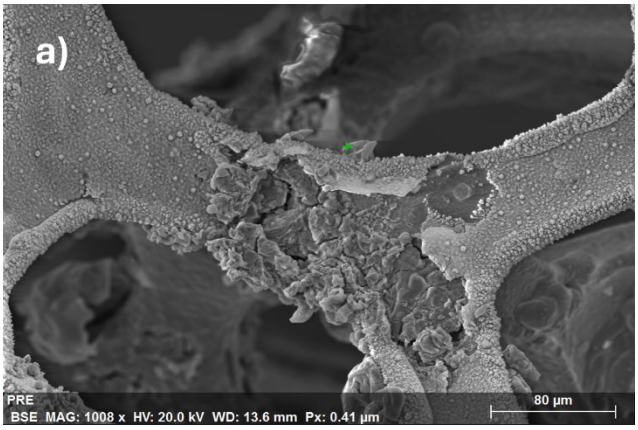

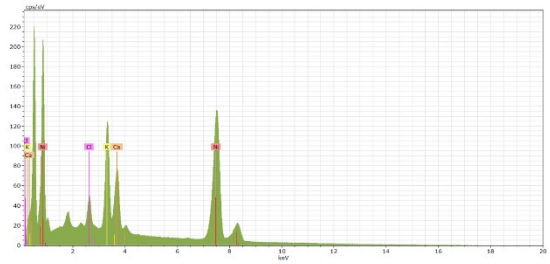

Element	atomic.%
Chlorine	4.801516
Potassium	16.78728
Calcium	11.59613
Nickel	66.81508

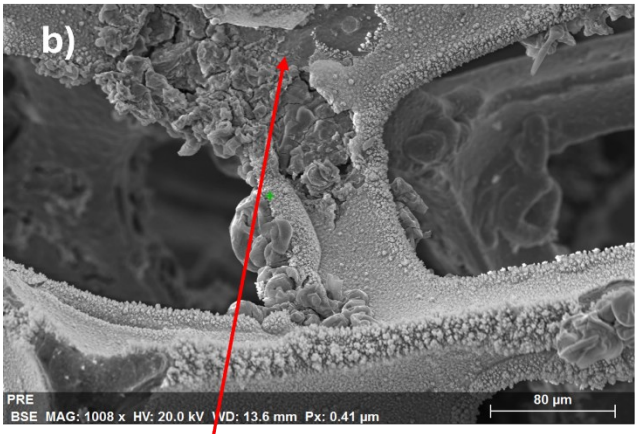

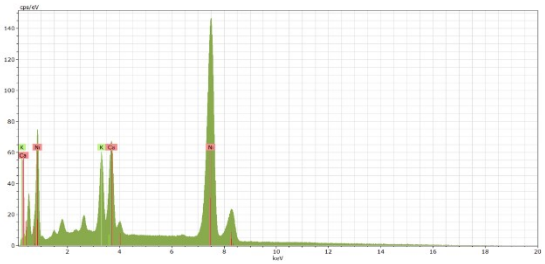

Element	atomic.%
Potassium	7.578912
Calcium	11.1452
Nickel	81.27589

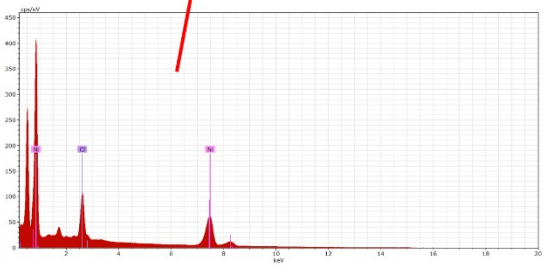

Element	atomic.%
Chlorine	10.34612
Nickel	89.65388

Fig. S13 SEM and EDS of $NiFe(OH)_2$ after testing in 1 M KOH & AbsOcean at 100 mA cm^{-2} for 10 h focusing on areas of corrosion.

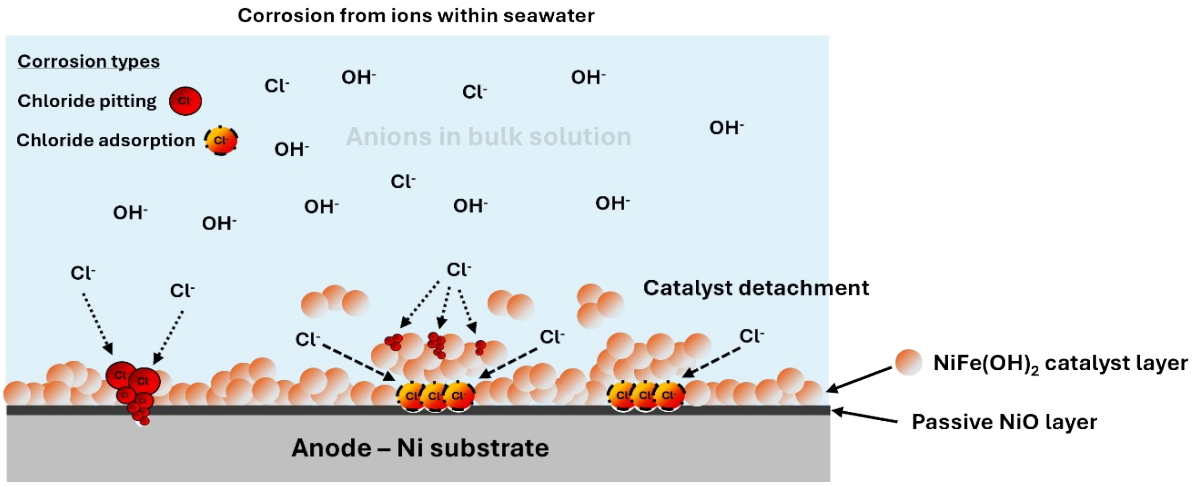

Fig. S14 Corrosion degradation mechanism from chloride ions in seawater.

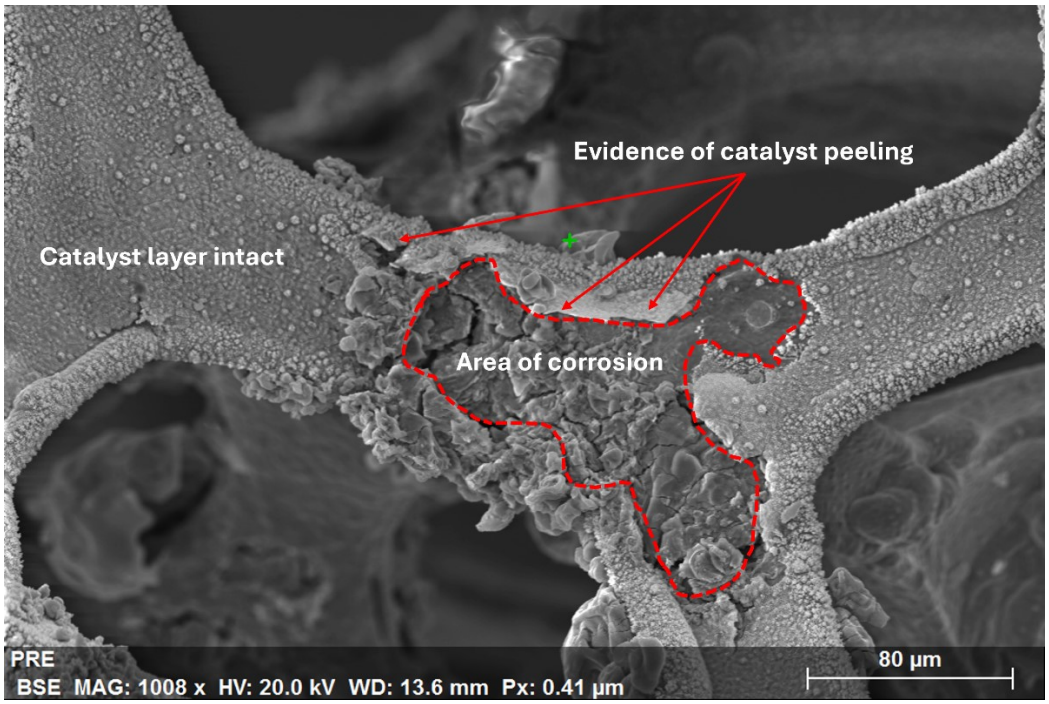

Fig. S15 Catalyst corrosion observed on $NiFe(OH)_2$ on nickel foam after electrolysis in 1 M KOH & AbsOcean at 100 mA cm^{-2} for 10 h focusing on areas of corrosion.

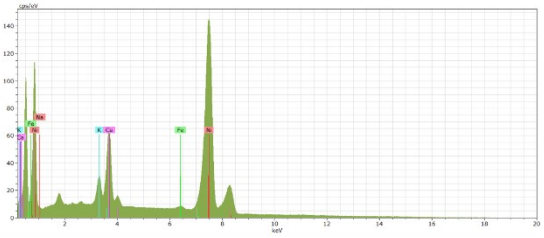

Element	atomic.%
Sodium	0.474074
Potassium	3.154733
Calcium	11.52679
Iron	1.309289
Nickel	83.53511

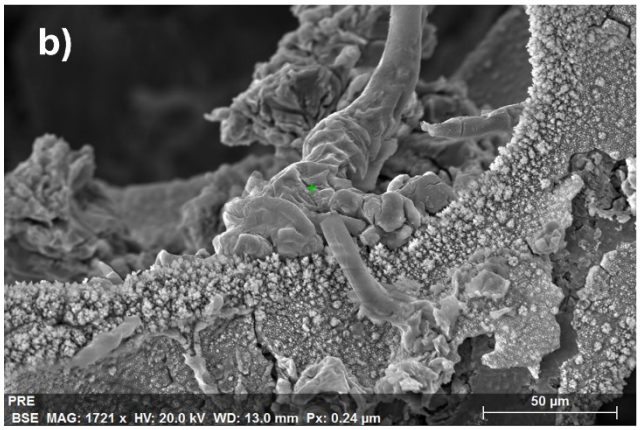

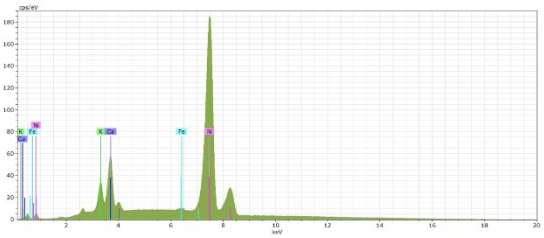

Element	atomic.%
Potassium	2.62486
Calcium	7.53889
Iron	1.521954
Nickel	88.3143

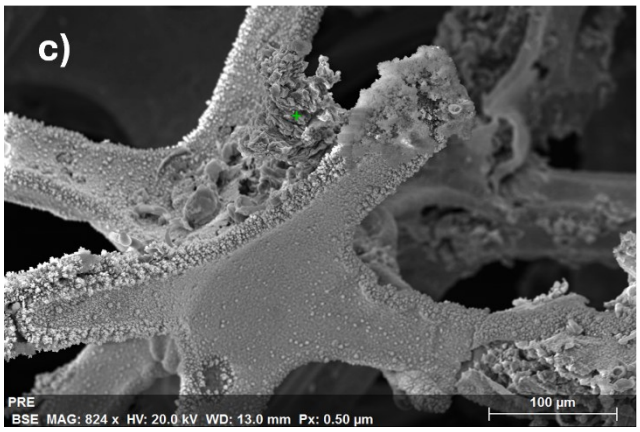

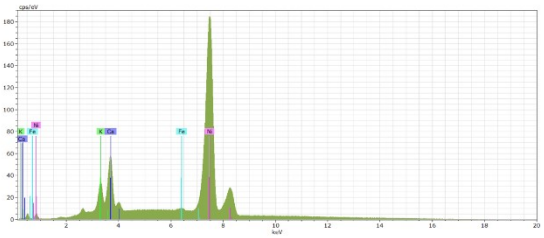

Element	atomic.%
Potassium	2.62486
Calcium	7.53889
Iron	1.521954
Nickel	88.3143

Fig. S16 SEM and EDS of $NiFe(OH)_2$ after testing in 1 M KOH & unfiltered seawater at 100 mA cm^{-2} for 10 h focusing on areas of corrosion.

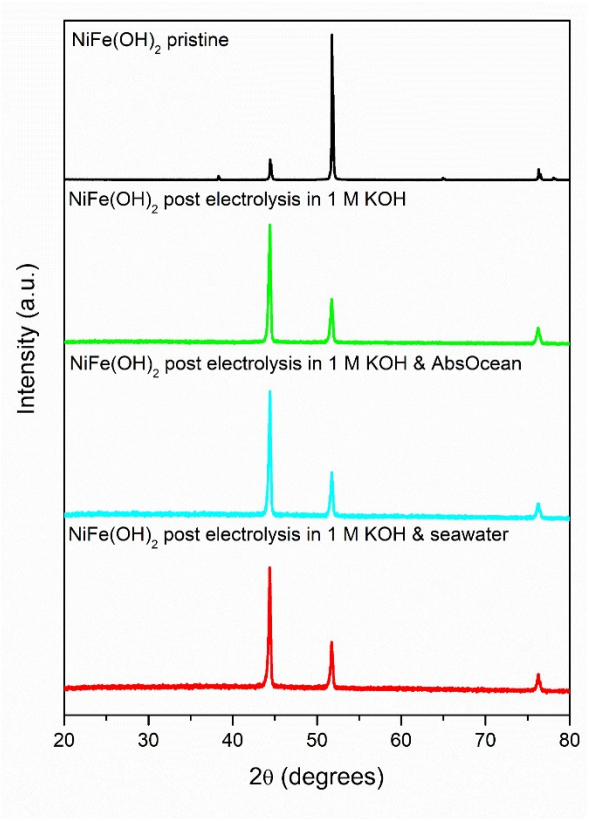

Fig. S17 XRD spectrum of $NiFe(OH)_2$ after 10 hours of electrolysis in various electrolytes using nickel foam as a substrate.

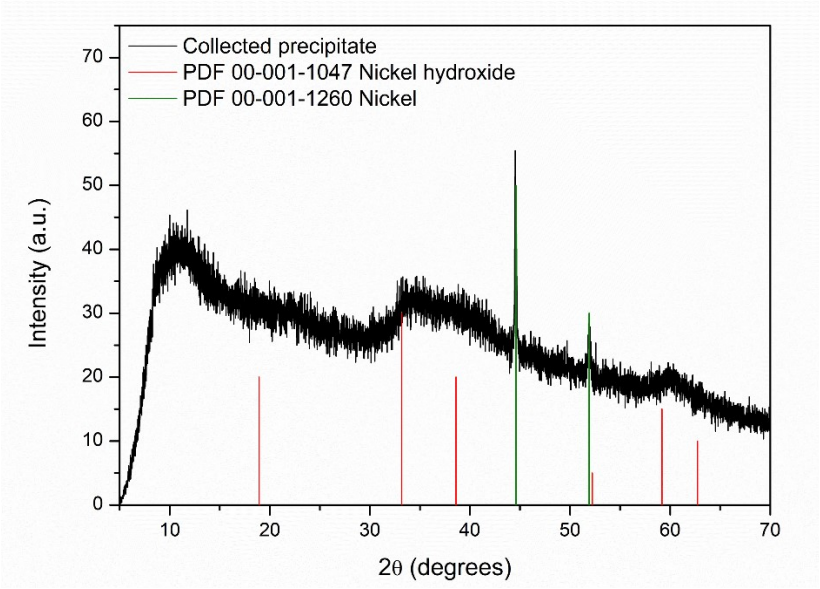

Fig. S18 XRD spectrum of green precipitate collected from the sample post-seawater electrolysis.

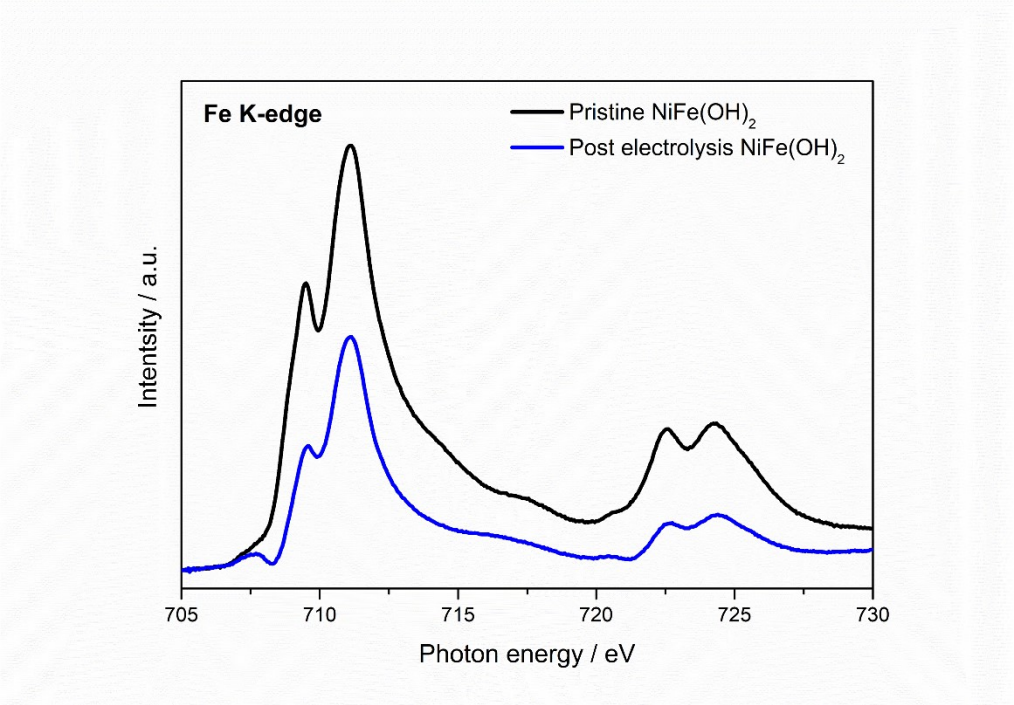

Fig. S19 Normalised Fe K-edge XANES spectra for $NiFe(OH)_2$ pristine vs after 4h of electrolysis at 50 mA cm^{-2}.

Table S4 Current densities and corresponding current densities under different conditions for $NiFe(OH)_2$ and similarly reported OER electrocatalysts.

OER Catalyst (reference)	**Electrolyte**	**Temp (K)**	**Current density**	**Overpotential**
$NiFe(OH)_2$ [This work]	1 M KOH	293	100, 500 and 1000 mA cm^{-2}	307, 329 & 400 mV
	1 M KOH & 0.5 M NaCl		100, 200, 250, 500, 750 & 1000 mA cm^{-2}	307, 322, 327, 351, 371 & 393 mV
	1 M KOH & unfiltered seawater		100 & ~200 mA cm^{-2}	359 & 387 mV
	1 M KOH	333	100, 250, 500, 750, 1000, 1200, 1500, 2000 & 2500 mA cm^{-2}	256, 276, 297, 311, 323, 333, 346, 367 & 392 mV
	1 M KOH & 0.5 M NaCl		100, 250, 500, 750, 1000, 1200, 1500 & 2000 mA cm^{-2}	238, 257, 278, 289, 305, 314, 328 & 341 mV

	1 M KOH & filtered seawater		100, 250 & 500 mA cm^{-2}	287, 309 & 331 mV
	1 M KOH & unfiltered seawater		100, 250, 500, 750, 1000 and 1200 mA cm^{-2}	294, 320, 347, 365, 383 & 392 mV
	1 M KOH & Alk-AbsOcean		100, 250, 500, 750, 1000, 1200, 1500 & 2000 mA cm^{-2}	234, 272, 305, 337, 349, 366, 384 & 409 mV
NiFe-LDH/CC [3]	1 M KOH & seawater	293	100 mA cm^{-2}	301 mV
Fe-NiMoSe@C [4]	1 M KOH & seawater	293	200 mA cm^{-2}	413 mV
	1 M KOH & 0.5 M NaCl		200 mA cm^{-2}	370 mV
(Ni/Fe/Mo)OOH [5]	1 M KOH & seawater	293	100 mA cm^{-2}	330 mV
Ni_3S_2/Co_3S_4 [6]	1 M KOH & seawater	293	100 mA cm^{-2}	360 mV
S-$NiMoO_4$@NiFe-LDH [7]	1 M KOH & seawater	293	100 mA cm^{-2}	315 mV
$NiCo_2O_4$ [8]	1 M KOH & seawater	293	10 mA cm^{-2}	293 mV
NiFe-LDH/Glassy carbon [9]	1 M KOH & 0.5 M NaCl	293	10 mA cm^{-2}	359 mV
Fe−$Ni(OH)_2/Ni_3S_2$/NF [10]	1 M KOH & 0.5 M NaCl	293	10 & 100 mA cm^{-2}	269 & 320 mV
Co−Fe−O−B/Glassy carbon [11]	1 M KOH & 0.5 M NaCl	293	10 mA cm^{-2}	294 mV
Ni_3S_2–MoS_2–Ni_3S_2 [12]	1 M KOH & 0.5 M NaCl	293	100 mA cm^{-2}	330 mV
$Fe_{0.05}$CoNi-LDH/NF [13]	1 M KOH & seawater	293	10 mA cm^{-2}	287 mV
Fe & P-$NiMoO_4$ [14] **(Fe and P doped)**	1 M KOH & seawater	293	10 mA cm^{-2}	120 mV

NiCoFe−Bi [15]	Alkaline seawater (pH: 14)	293	500 mA cm^{-2}	329 mV
			1000 mA cm^{-2}	336 mV
Cr_2O_3-CoO_x [16]	Neutral seawater	293	100 mA cm^{-2}	420 mV
S–Cu_2O–CuO [17]	1 M KOH + 0.5 M NaCl	293	500 mA cm^{-2}	420 mV
Ru-CoO_x [18]	1 M KOH + seawater	293	100 mA cm^{-2}	630 mV
Ni_3S_2/Fe-NiP_x [19]	1 M KOH + seawater	293	500 mA cm^{-2}	336 mV

References

[1] O. Horner, E. L. Gyenge and D. P. Wilkinson, ECS Meeting Abstracts, 2024, MA2024-01, 1724–1724.

[2] A. Kisyov and Y. Ivanov, GEOPHYSICAL APPROACH FOR MONITORING SALTWATER INTRUSION IN COASTAL AQUIFERS, 2016, vol. 59.

[3] M. L. Frisch, T. N. Thanh, A. Arinchtein, L. Hager, J. Schmidt, S. Brückner, J. Kerres and P. Strasser, ACS Energy Lett, 2023, 8, 2387–2394.

[3] Dong, G. et al. (2021) 'NiFe-layered double hydroxide arrays for oxygen evolution reaction in fresh water and seawater', Materials Today Energy, 22, p. 100883. doi:10.1016/j.mtener.2021.100883.

[4] Xu, X. et al. Fe-Doped and Carbon Composite Multiphase Hetero-structured Catalysts Based on the Ion-Exchange Strategy for Seawater Electrolysis. ACS Sustain Chem Eng 11, 15338–15349 (2023).

[5] L. Xu, Y. Dong, W. Xu and W. Zhang, Catalysts, 2023, 13, 924.

[6] Wang, C. et al. Heterogeneous bimetallic sulfides based seawater electrolysis towards stable industrial-level large current density. Appl Catal B 291, 120071 (2021).

[7] H. Wang, L. Chen, L. Tan, X. Liu, Y. Wen, W. Hou and T. Zhan, J Colloid Interface Sci, 2022, 613, 349–358.

[8] Yang, J. et al. Quench-Induced Surface Engineering Boosts Alkaline Freshwater and Seawater Oxygen Evolution Reaction of Porous NiCo2O4 Nanowires. Small 18, 2106187 (2022).

[9] Dionigi, F. et al. (2016) 'Design criteria, operating conditions, and nickel–iron hydroxide catalyst materials for selective seawater electrolysis', ChemSusChem, 9(9), pp. 962–972. doi:10.1002/cssc.201501581.

[10] Cui, B. et al. (2020) 'Heterogeneous lamellar-edged Fe-Ni(OH)2/NI3S2 nanoarray for efficient and stable seawater oxidation', Nano Research, 14(4), pp. 1149–1155. doi:10.1007/s12274-020-3164-3.

[11] Gupta, S. et al. (2020) 'Highly efficient and selective metal oxy-boride electrocatalysts for oxygen evolution from alkali and Saline Solutions', ACS Applied Energy Materials, 3(8), pp. 7619–7628. doi:10.1021/acsaem.0c01040.

[12] Y. Li, X. Wu, J. Wang, H. Wei, S. Zhang, S. Zhu, Z. Li, S. Wu, H. Jiang and Y. Liang, Electrochim. Acta, 2021, 390, 138833.

[13] Gupta, A., Sadhanala, H. K. & Gedanken, A. Iron doped cobalt nickel layered double hydroxide supported on nickel foam as a robust electrocatalyst for highly efficient water oxidation in alkaline sea water. Electrochim Acta 470, 143269 (2023).

[14] Zhang, D., Wang, Y., Du, X. & Zhang, X. Iron and phosphorus dual-doped NiMoO4 with nanorod structure as efficient oxygen evolution catalyst in alkaline seawater. Int J Hydrogen Energy 49, 1387–1398 (2023).

[15] Zhang, X. et al. (2023) 'Stable seawater oxidation with a self-healing oxygen-evolving catalyst', Inorganic Chemistry Frontiers, 10(10), pp. 3103–3111. doi:10.1039/d3qi00470h.

[16] Guo, J. et al. (2023) 'Direct seawater electrolysis by adjusting the local reaction environment of a catalyst', Nature Energy [Preprint]. doi:10.1038/s41560-023-01195-x.

[17] Haq, T. ul and Haik, Y. (2022) 'S doped CU2O-Cuo nanoneedles array: Free standing oxygen evolution electrode with high efficiency and corrosion resistance for seawater splitting', Catalysis Today, 400–401, pp. 14–25. doi:10.1016/j.cattod.2021.09.015.

[18] Wu, D. et al. (2021) 'Ultralow RU incorporated amorphous cobalt-based oxides for high-current-density overall water splitting in alkaline and seawater media', Small, 17(39). doi:10.1002/smll.202102777.

[19] Luo, X. et al. (2022) 'Spherical ni3s2/fe-nipx magic cube with Ultrahigh Water/seawater oxidation efficiency', Advanced Science, 9(7). doi:10.1002/advs.202104846.